J Mater Sci: Mater Med (2009) 20:2025–2034
DOI 10.1007/s10856-009-3764-7

Low temperature fabrication of high strength porous calcium phosphate and the evaluation of the osteoconductivity

Xianzhu Yu · Shu Cai · Guohua Xu · Wei Zhou · Dongmei Wang

Received: 19 October 2008 / Accepted: 24 April 2009 / Published online: 8 May 2009

Abstract Porous NaO_2–MgO–CaO–P_2O_5 bioglass doped beta-tri-calcium phosphate (β-TCP) bioceramic possessing high mechanical properties and well pore structure with high porosity and high pore connectivity has been prepared through dipping method with the porous polyurethane as the pore forming template. The sintering mechanism and the mechanical properties of the bioglass doped β-TCP scaffold have been investigated by the X-ray diffraction (XRD) analysis, Scanning electron microscope (SEM) and thermal differential analysis (DTA). The scaffold's in vivo osteoconductivity has been evaluated by implantation of scaffolds into the femurs of New Zealand rabbits. The results show that the porous structure can achieve the densification process at a low temperature about 950°C by a solid solution sintering mechanism and hence dense macropore scaffold with a compressive strength of 4.32 MPa when the porosity is 75% has been obtained. The in vivo test shows that the Na_2O–MgO–CaO–P_2O_5 bioglass doped porous β-TCP bioceramic has a relatively fast bone formation after implantation; after 1 month implantation new deposited bone tissue has been detected on the strut of the porous scaffold and degraded particles also has been found on the surface of the new formed bone. After 6 months implantation the porous scaffold has been thoroughly covered with new formed bone. Results show that the Na_2O–MgO–CaO–P_2O_5 bioglass doped porous β-TCP bioceramic is potential bone tissue engineering scaffold for orthopedic use.

X. Yu · S. Cai · W. Zhou · D. Wang
Key Laboratory for Advanced Ceramics and Machining Technology of Ministry of Education, Tianjin University, Tianjin 300072, People's Republic of China

X. Yu
China Nation Academy of Nano Technology and Engineering, Tianjin 300457, People's Republic of China

G. Xu (✉)
Shanghai Changzheng Hospital, Shanghai 200003, People's Republic of China
e-mail: guohuaxumail@gmail.com

1 Introduction

Calcium phosphate ceramics are considered among the most promising materials for bone tissue engineering because their bone-like composition and mechanical properties [1, 2]. And the biodegradation properties of these materials allow for efficient bone tissue engineering as they can promote apatite formation and simultaneously deliver growth factors for osteoinduction.

Calcium phosphate exists in various phase depending on temperature and partial pressure of water. The included beta-tri-calcium phosphate (β-TCP) is a resorbable phase and exhibits good biocompatibility. However, β-TCP is difficult to sinter; shows poor mechanical strength and low resistance to crack-growth propagation [3] for orthopedic applications due to the phase transformation of β phase to α phase.

Porous calcium phosphate biomaterials is a series of very important materials in the bone tissue engineering that the macro pore ranged from 100 μm to 500 μm allowed the bone tissue grow into the material, and the porous scaffold should degrade by advancing bone growth [4]. Therefore, the porous structure of a synthetic bone should resemble the morphology of the natural one being replaced. In this regard, size and distribution of pores and their interconnection become quite important. There has been reported that the pore interconnectivity plays an important role in

the in vivo bone growth rather than the porosity. There exist several methods to prepare porous bone tissue engineering scaffolds such as freeze casting [5], solid free form fabrication method (SFF) [6] or three dimensional printing [7]. The polyurethane dipping method seems a simple method to gain high porosity and three dimension interconnected pore structure when compared to the above methods. But there presents a compromise between the high qualities of pore structure and the high mechanical properties no matter which method. Especially the β-TCP bioceramic that posses negative high temperature phase transformation from β to α phase when sintering that may influence the mechanical properties of the material [8]. Many researches have been reported aiming to improve the sintering property of the β-TCP by inducing a variety of sintering addictives into the β-TCP matrix during the sintering [8–14]. Our previous study [15, 16] showed that a bioglass with the composition of Na_2O–MgO–CaO–P_2O_5 that the chemical composition is similar to nature bone when compared to other bioglass used for bone tissue engineering [17] in can significantly decrease the densification temperature of the β-TCP bioceramic and improve the mechanical properties of both the dense porous pyrophosphate glass reinforced β-TCP biomaterial. In the present study the porous scaffold reinforced by Na_2O–MgO–CaO–P_2O_5 bioglass has been prepared through dipping method and the reinforcement mechanism has been well discussed and animal experiment has been performed in New Zealand rabbits to test the material's osteoconductivity.

2 Materials and methods

2.1 Preparation of the porous scaffold

The β-TCP powder was synthesized through solid reaction method with the analytical regent $CaHPO_4 \cdot 2H_2O$ and $CaCO_3$ as the starting material. After well ball milled and grounded the mixed powders are heated to form fine crystallized β-TCP powder. The synthesis route is as following: heating at 400°C for 0.5 h and then calcined at 900°C for 1 h.

The Na_2O–MgO–CaO–P_2O_5 based bioglass was prepared by quenching a high temperature (1000°C) glass solution into cold water. The starting materials are analytical regent $CaCO_3$, $MgCO_3 \cdot 5H_2O$, Na_2CO_3 and $CaHPO_4 \cdot 2H_2O$. After mixed with a composition of $62.04P_2O_5$–$14.68CaO$–$13.00MgO$–$10.28Na_2O$ by a weight ratio, the powders were heated and quenched to cooled glass particles and then were grounded and meshed to about 150 μm for a further use.

Porous Na_2O–MgO–CaO–P_2O_5 bioglass doped β-tricalcium phosphate (BG/β-TCP) biomaterial was fabricated by dipping method with polyurethane as the pore template. The polyurethane was pre-treated with 10% NaOH solution to eliminate the closed pore among the porous structure and then washed by large amount of distilled water and then dried below the temperature of 80°C. The ceramic slurry was fabricated by ball milling a mixture of bioglass (BG) and β-TCP by a weight ratio of 20:80 with the distilled water as the liquid phase for about 30 min. The PVA and ammonium salt of polycyclic were added as the adhesive and dispersive agent. After the ball milling, the polyurethane samples were dipped into the slurry and were squeezed repetitively to eliminate the residual slurry. The processed green porous samples were dried at the room temperature for about 24 h and then were sintered in a muffle furnace at the temperature of 950°C for 2 h. The heating rate bellow the temperature of 600°C was carefully controlled with a heating rate about 50°C/h for the elimination of polyurethane.

2.2 In vivo testing

Cylindrical samples, 2 mm in diameter and 2 mm in length, were implanted in the femurs of 12 adult male New Zealand rabbits that have been averagely divided into four groups and every group 3 rabbits. Both femurs were used. The samples were pure porous β-TCP and 20% BG doped β-TCP scaffolds.

General anesthesia was induced with an i.m. injection of 44 mg/kg ketamine and 3 mg/kg xylazine, and assisted ventilation (O_2:11/min; N_2O: 0.41/min; isofluorane: 2.5–3%). The distal femurs and middiaphyses were exposed and 2 defects with a 2 mm diameter were drilled at low speed and under continuous saline irrigation in the trabecular (distal femurs) and cortical (middiaphyses) bone of the right and left femurs. Pure porous β-TCP samples and BG doped β-TCP samples were transversally implanted in the left femur of all rabbits, while BG doped β-TCP samples were positioned in the right femurs; finally, the skin was sutured layer by layer. Antibiotic therapy was administered preoperatively, immediately after surgery and after 24 h. Analgesics were prescribed in the immediate postoperative period. Seven days prior to sacrifice, the animals received an i.m. injection of oxytetracycline (30 mg/kg). After 4, 8, 12 and 24 weeks, one group of animals was sacrificed with an overdose of pentobarbital sodium. The implants were harvested with surrounding tissues and fixed in 4% buffered formaldehyde (pH = 7.4) immediately.

The fixed implants were washed with phosphate buffer solution (PBS), dehydrated in a series of ethanol solutions (70%, 80%, 90%, 95%, and 100%) and embedded in methyl methacrylate (MMA). Then the samples were dried

at a temperature below 100°C and sprayed with Au for further scanning electron microscope (SEM) analysis.

2.3 Characterization of the materials

The porosity of the BG/β-TCP scaffolds was determined by mercury porosimetry (AutoporeII, 9220). Four specimens were selected to determine porosity with an error of less than 1% of the measured porosity value.

Identification of the crystalline phases of the bioglass powders and β-TCP/BG samples was carried out by X-ray diffraction analysis (D/MAX-2500). The diffraction patterns were collected with Cu Kα radiation over an angular range of 10–60° (2θ values). Microstructure observations of the porous structures were determined by environmental scanning electron microscope (ESEM) (Model XL30).

The compressive strength was evaluated in cylindrical specimens ($\Phi = 6$ mm, heigh = 10 mm) at a crosshead speed of 1 mm/min.

3 Results and discussion

3.1 Compressive strength and porosity evolution

Table 1 shows the evaluation of the porosity and compressive strength of the porous β-TCP with different bioglass content. The results show that with the increment of the bioglass content, the porosity of the porous scaffold shows a small increase from 65% to 73%, and the compressive strength of the porous β-TCP matrix can be significantly improved by a increment of the bioglass content below 20 wt%, but above 20 wt% the compressive strength shows a small decrease.

3.2 XRD phase analysis

Figures 1 and 2 show the XRD patterns of the fabricated bioglass and the 20 wt% bioglass doped β-TCP porous matrix, respectively. From Fig. 1 can see that the main phases of the quenched bioglass are the orthophosphate, metaphosphate, and polyphosphate salts, but no pyrophosphate phases can be found. It can be verified that these phosphate salts [18] are chemical stable when touch with water and have no negative influence on the properties of the slurry hence will not influence the processing procedure of the porous scaffolds.

After a fine analysis to the XRD curves of the 20 wt% BG doped β-TCP matrix, a small shift from the small angle to a large angle of the β-TCP curve has been found when comparing to the standard PDF card of the β-TCP phase and it closely matched to a phosphate salt phase $Ca_9MgNa(PO_4)_7$. For further understanding the appearance of the phase $Ca_9MgNa(PO_4)_7$ in the β-TCP matrix, the calculation of lattice content of pure β-TCP matrix and 20 wt% BG doped β-TCP has be conducted. β-TCP belongs to the R3CH space group and has a hexagonal crystal structure [4]. The formulas used are as following:

$$d_{hkl} = 0.9\lambda/(F_{WHM}\cos\theta)$$

$$d_{hkl} = \left[(4/3a^2)\left(h^2 + k^2 + hk\right) + \left(l^2/c^2\right)\right]^{-1/2}$$

where the d_{hkl} is the crystalline size; F_{WHM} is the full width at half maximum for diffraction peak and the θ is the diffraction angle, and the lattice constants of the β-TCP matrix is calculated through the choice of three peaks corresponding to the plans of (012), (104) and(110) in the small angle scale. To compare, the average parameter values of the *a*-axis and *c*-axis were calculated with the *a*-axis and *c*-axis values got from the three plans' d_{hkl}. The results were shown in the following Table 2.

From the result can conclude that when 20 wt% bioglass has been doped into the β-TCP structure both the *a*-axis and the *c*-axis has been lengthened indicting that the solid solution of the ions in the bioglass into the dense β-TCP structure has occurred by the interstitial form but not the form of substitution since the ion radium of the Mg^{2+} (0.075 nm) and Na^+ (0.098 nm) are both smaller than the Ca^{2+} ion(0.105 nm) and as a result the new phase of $Ca_9MgNa(PO_4)_7$ has been formed.

3.3 Low temperature sintering of the high strength porous structure

It is well accept that the phase transformation of β-TCP to α-TCP with a volume change of about 4% is a critical factor influencing the densification of the β-TCP. Many researches have been conducted to improve the sintering ability by introducing various sintering addictives such as the MgO, Al_2O_3, SiO_2, TiO_2, ZrO_2, $Ca_2P_2O_7$, etc. [8–14] and showed both positive or negative effects on the

Table 1 Average porosity and compressive strength of the bioglass doped β-TCP

Bioglass content (wt%)	0	10	20	30
Porosity	65% ± 8%	70% ± 7%	75% ± 10%	73% ± 10%
Compressive strength (MPa)	1.22	1.43	4.32	4.25

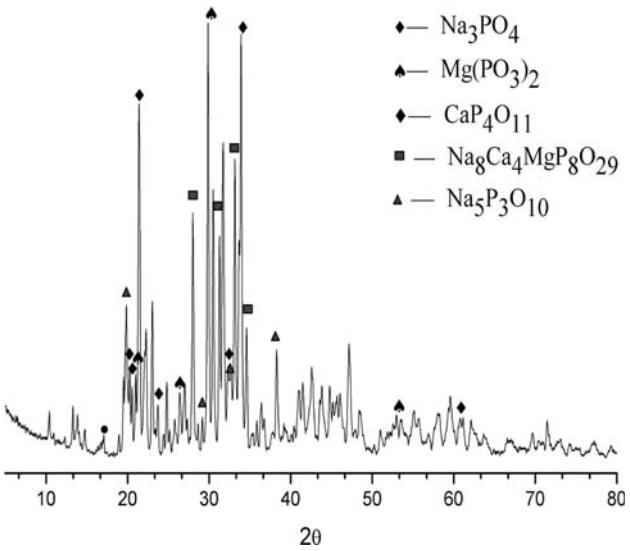

Fig. 1 XRD pattern of the quenched bioglass

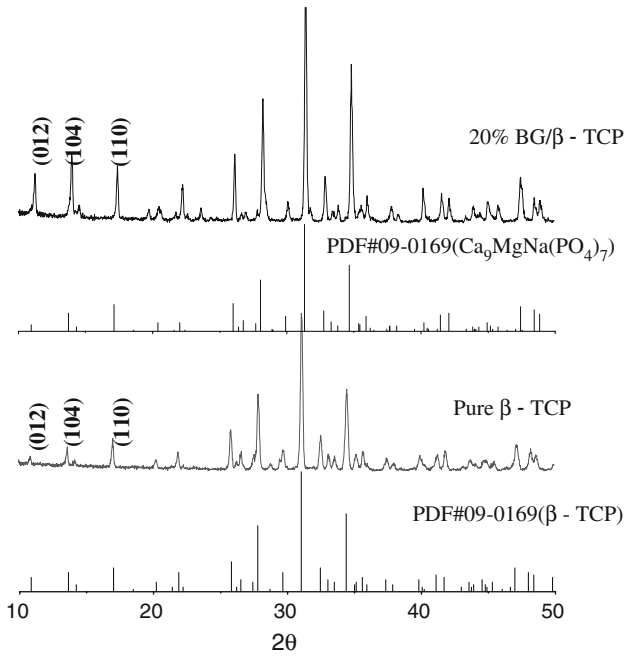

Fig. 2 XRD curves of the pure β-TCP and 20 wt% bioglass doped β-TCP

Table 2 The calculation results of the *a*-axis and *c*-axis values of the pure β-TCP and 20 wt%BG/β-TCP

β-TCP				20 wt% BG/β-TCP			
hkl	d_{hkl} (Å)	a (Å)	c (Å)	hkl	d_{hkl}	a (Å)	c (Å)
(012)	7.9833	10.1958	37.3717	(012)	8.1407	10.4364	37.4760
(104)	6.4173	10.1958	37.3717	(104)	6.5048	10.4364	37.4760
(110)	6.1796	12.3591	37.3717	(110)	6.2470	12.4941	37.4760
Average a, c value (Å)		10.9169	37.3717			12.1223	37.4760

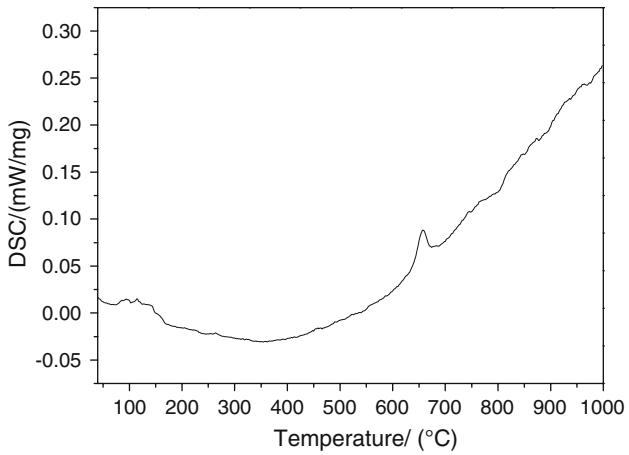

Fig. 3 DTA curve of the quenched bioglass

mechanical properties of the β-TCP matrix. This research shows that the addition of a small amount of Na_2O–MgO–CaO–P_2O_5 bioglass into the β-TCP structure can significantly reduce the sintering temperature to 950°C that had especially facilitated the improvement of the mechanical properties of the porous β-TCP matrix with a increase of the bioglass content (Table 1). This can be explained by a liquid phase sintering mechanism during the sintering process that on one hand, crack defects formed in the drying process due to the different shrinking rate between the wet β-TCP slurry and the porous polyurethane matrix can be repaired effectively by the formed liquid phase. Figure 4 shows the wall structure of polyurethane and the porous β-TCP ceramics. In the Fig. 5c, microcracks can be clearly observed on the surface of the pore wall structure with a low bioglass addition (10 wt % BG), but Fig. 4b shows a smooth and dense wall structure while the BG content reached to 20 wt%. These defects are large enough that samples can not be sintered to a dense structure with the solid phase sintering mechanism either by elevating the sintering temperature or by elongating sintering time. The presence of the lower viscous liquid glass (Fig. 3) can play a role of mass transfer media in the large crack defects when the temperature has reached a certain temperature. When the temperature increased, the bioglass would become more viscous and would assemble in the large crack defects owing to gravity during the sintering and then the ions can diffuse in the low viscosity bioglass phase with a faster diffusion speed comparing to that in the solid phase. With this mechanism, the micro cracks could be well repaired during the sintering. Figure 4b shows the smooth pore wall structure of the 20 wt% BG/β-TCP microscopy that can not detect the micro cracks as shown in Fig. 4c with 10 wt% bioglass content (10 wt% BG/β-TCP).

And on the other hand, the promotion effect of the densification process and consequently the significant

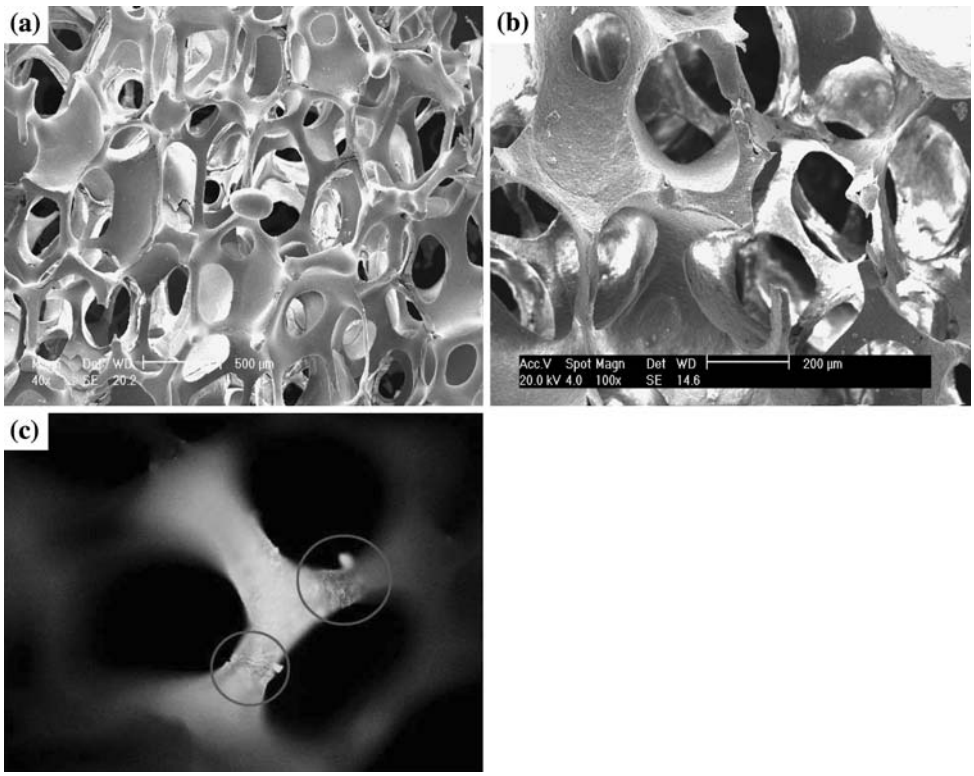

Fig. 4 SEM micrographs of the porous scaffold structure: **a** polyurethane; **b** 20 wt% bioglass doped β-TCP; **c** 10 wt% bioglass doped β-TCP

improvement of the mechanical property are also due to the solid solution sintering mechanism of the Na^+, Mg^{2+}. The XRD curve of the porous β-TCP in Fig. 2 shows that, the prime phase of the bioglass doped β-TCP structure is β-TCP and is accompanied with an additional phase of $Ca_9MgNa(PO_4)_7$. The presence of the new phase of $Ca_9MgNa(PO_4)_7$ which is due to the solid solution of Na^+, Mg^{2+} ions into β-TCP structure during the sintering may produce a lot of defects thus cause a disequilibrium of ion concentration and vacancy concentration and hence has provided a sintering driving force resulting in the promotion of the mass transfer process and furthermore the densification of the β-TCP at a low temperature. This can not only avoid the phase transformation of the β to α phase, but also has probably strengthen the grain boundary by the formation of a chemical bond between the grains due to the formation of the $Ca_9MgNa(PO_4)_7$ phase that leads to more transgranular fracture as shown in the Fig. 6b–e.

3.4 Microstructure analysis

Figure 4 shows the macro pore structure of the porous β-TCP scaffolds. It can be seen that high porosity and interconnect pore structure with the pore size of 100–500 µm has gained by employing the porous polyurethane as the template matrix. From the surface morphology of the pore structure (Fig. 6a) the clear grains and grain boundaries could be found and the average small grain size is about 2 µm, but some grains with the grain size larger than 10 µm has also been observed that can be defined as the abnormal grain growth which is commonly seen in the liquid phase sintering system [19]. It has been well accepted that the presence of the secondary phase mostly the sintering addictives in the boundaries may play a role of inhibition on the grain growth and finally resulting in a small average grain size [20]. In this study the small average grain size has gained due to the inhibition effect of the second phase bioglass in the grain boundary during sintering. Figure 4e shows that the fracture of the large crystals is mainly the transgranular fracture that this might due to the chemical bond on the boundary and also the strengthen effect of the residual stress formed by the little lattice volume expansion as discussed following.

Figure 5b, c–e show the fracture faces of the macro pore wall structure with bioglass content of 30 wt% and 20 wt%, respectively. It can be seen that with an increase of bioglass amount more ladder-like fracture structures were detected as shown in Fig. 5b, c. When the glass content is elevated to 30 wt%, the fracture face has become to the structure that likes planes of fibers assembled layer by layer and more cracks have been found among the fracture faces (white marrows). The XRD analysis of the bioglass doped β-TCP shows that ions of Na^+ and Mg^{2+} are the interstitial ions in the β-TCP crystals and as a result the a-axis and c-axis values have increased. This would lead to a small volume expansion of the β-TCP crystals that residual strength has formed among the grain boundary.

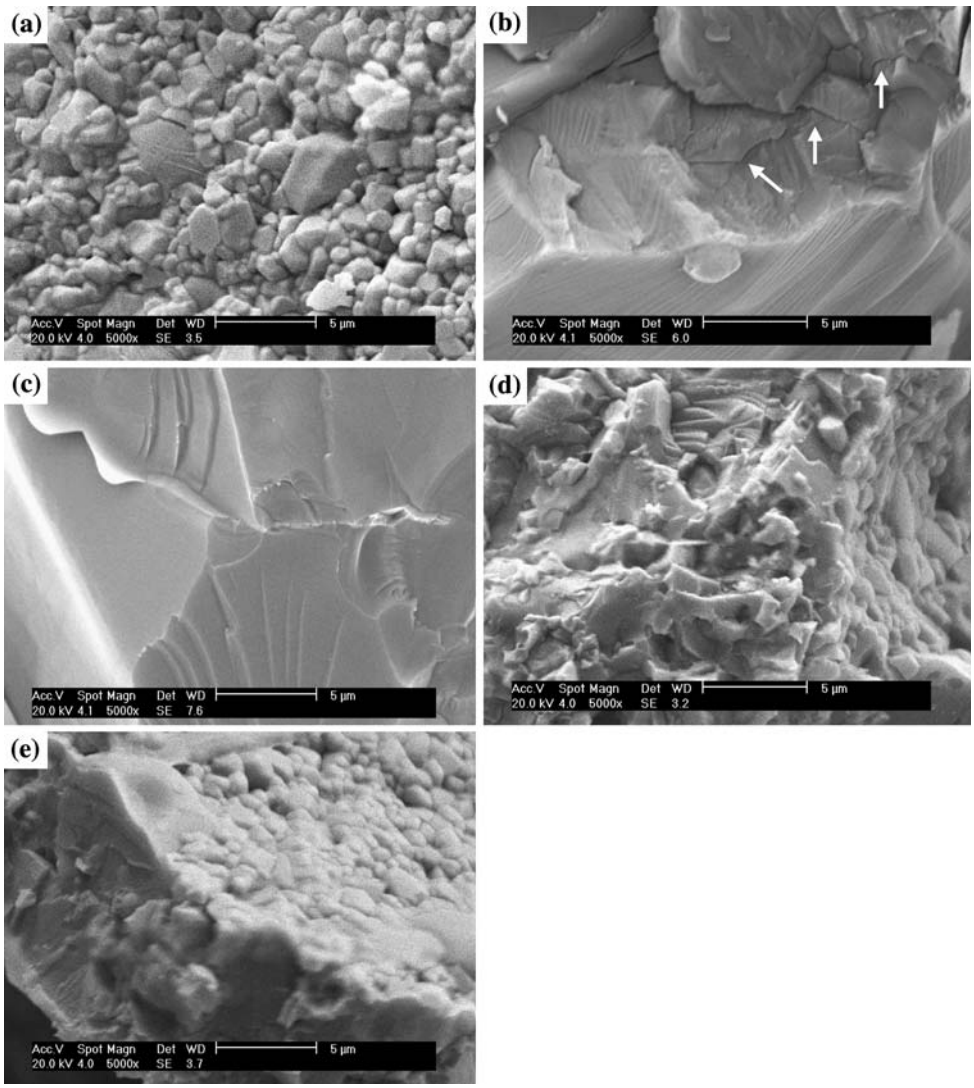

Fig. 5 Surface and fracture face morphology of the pore wall structure of the porous bioglass doped β-TCP matrix: surface morphology (**a**); fracture face morphology: (**b**) 30 wt% BG content and (**c**)–(**e**) 20 wt% BG content

This presence of the residual strength would improve the grain boundary property that may induce more intergranular fracture to transgradular fracture when the bioglass content is below appropriate point as shown in the Fig. 5b–e. But when the incorporated bioglass increases to a high content the solid solution mechanism would show negative effects on the mechanical properties of the β-TCP matrix due to that too much Mg^{2+} and Na^{+} ions have incorporated into the β-TCP structure as shown in the compressive strength result in Table 1 that this effect can be similar to the volume change of the phase transformation of β to α. in the tri-calcium phosphate ceramics. And while the fracture has occurred the residual strength would release resulting in the formation of cracks as shown in the Fig. 5b.

3.5 In vivo test

Figures 6, 7, 8, and 9 show the SEM micrographs and light photomicrographs of tissue staining of the porous scaffolds implanted into the femurs of the rabbits with different time. From photo micrographs the Fig. 6e, f of porous scaffold after implanted for 1 month can see that pore strut has become loosing and a thin film of unconnected new formed bone (white marrows) has formed on the surface of the scaffold strut and degraded particles indicated by gray marrows also can be detected. Among the degraded particles new small amount of new formed bone tissue also has been detected. From the SEM micrograph of the implanted scaffolds Fig. 6a can see that a layer of new formed bone can be detected on the surface of the strut. By a magnification insight of the new formed bone as shown in Fig. 6b, can see that the new bone apatite layer has deposited in the fibrous extra cellular matrix. From the magnification insight of the macropore structure without the new bone as shown in the Fig. 6e can see that the structure of the β-TCP surface has become loosening and some round shape like or polygonal like bone cells [21] with fibrous extra cellular matrix

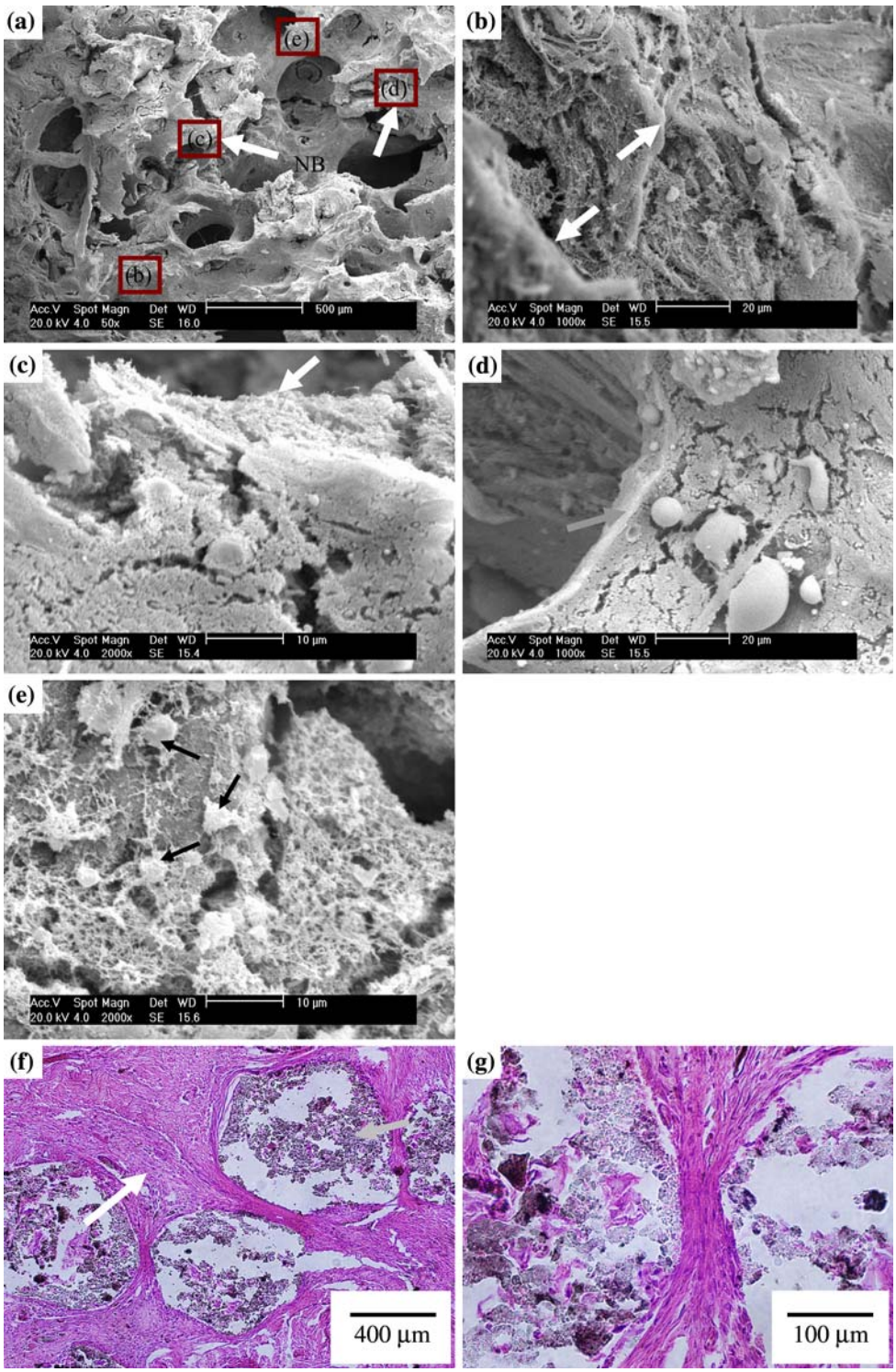

Fig. 6 SEM micrographs of the scaffolds after implantation for 1 month showing the new bone formation and degradation: **a–c** bone formation, white marrows; (**d**) degradation particles, *gray marrows* (**e**) bone cells, *black marrows* and light photomicrographs (**f**, **g**)

also has been found on the surface of the bioceramic. In some area of the surface of the new bone, spherical degraded β-TCP particles have been observed. Figure 7 shows the morphology of the material after implantation for 3 months. It can be seen that the porous structure has been covered with blocks and films of new formed bone and the deposited apatite has become thicker. From the SEM micrograph as shown in Fig. 7a–c can see that the new deposited apatite was large plate like with fibrous tissue and degraded particles inside. After 6 months implantation, the SEM micrograph as shown in Fig. 8 shows that the porous structure has been thoroughly covered with the new formed bone. The magnification insight of the new bone as shown in Fig. 8b indicated that

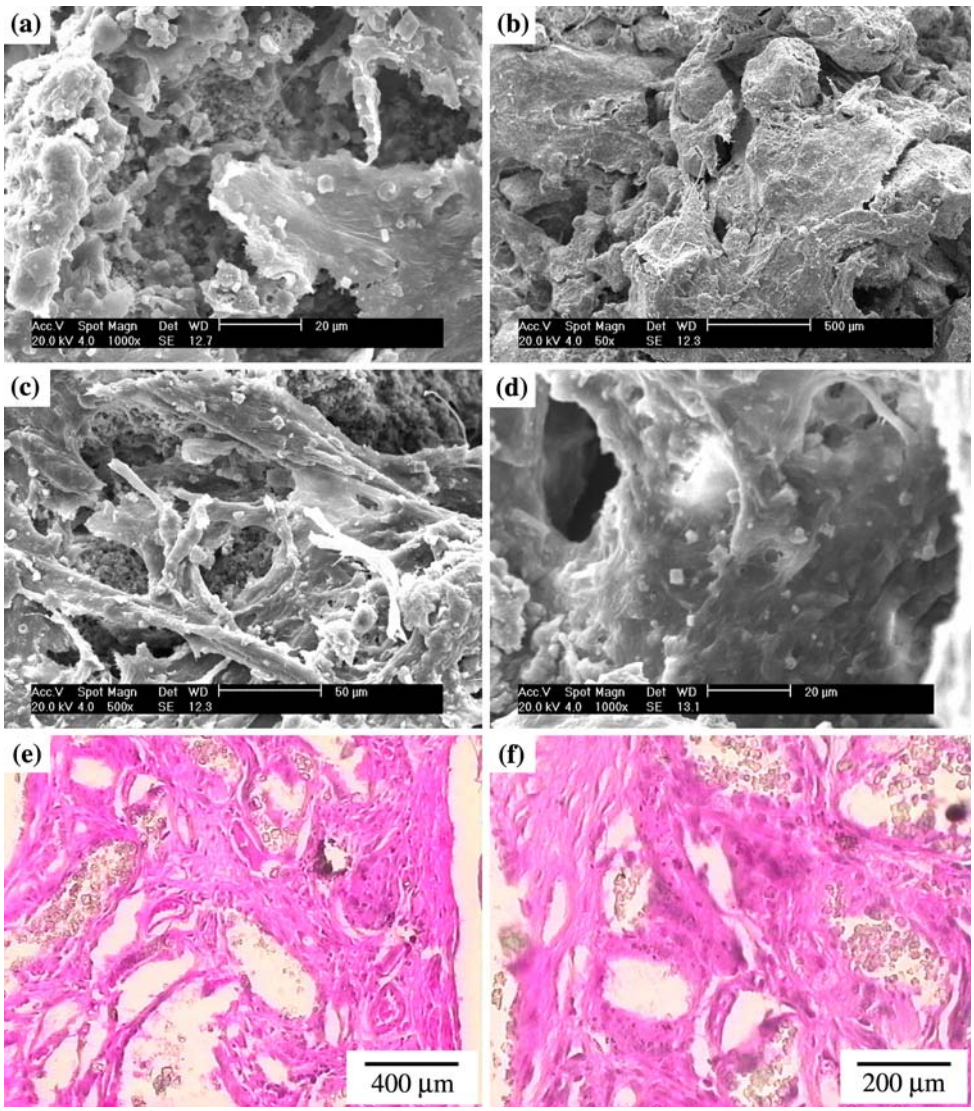

Fig. 7 SEM micrograph (**a**–**d**) and light photomicrographs (**e**) and (**f**), (new bone: white marrows, degraded particles: gray marrows) of the scaffold implanted after 3 months

the bone was compound with large amount of fibrous tissues inside and degraded spherical particles on the surface.

As a comparison, the 20 wt% bioglass doped β-TCP porous structures without the in vitro cell culture implanted for 6 months were displayed in the Fig. 9. It can be seen that after implantation of 6 months, a lot of fibrous tissues had grown into the porous structure (Fig. 9b) and the material had collapsed and degraded into blocks and spherical participles (Fig. 9c).

It has been well accepted that the interconnectivity of the macro pore of the biomaterial is essential for the bone tissue ingrowths [22]. The interconnected macro pores can allow the bone tissue grow into the material and the porous pore structure can provide the environment for ions to dwell to a high ions concentration comparing to the dense samples that ions may be easily flowed away by the fluid. Figure 6 shows that after 1 month implantation there has been a certain amount of new bone formed on the surface of the porous β-TCP structure. And after 6 months the porous structure has thoroughly been covered with the new formed bone. This fast bone formation may be partly caused by the high interconnectivity of the porous bioglass doped β-TCP scaffolds.

This study shows that a composition of Na_2O–MgO–CaO–P_2O_5 bioglass has not influenced the material's in vivo biocompatibility and after 1 month implantation new bone has deposited on the surface of the β-TCP and with the elongation of the implantation time the amount of the new formed bone increased. It has been reported that the high concentration of the calcium ion can induce bone formation in vivo [23], and this is perhaps one factor of promoting the increasing of bone formation amount due to the high calcium ions concentration resulted by the porous structure. There is also research report that the crystal structure and chemical stability of the β-TCP has significantly influenced

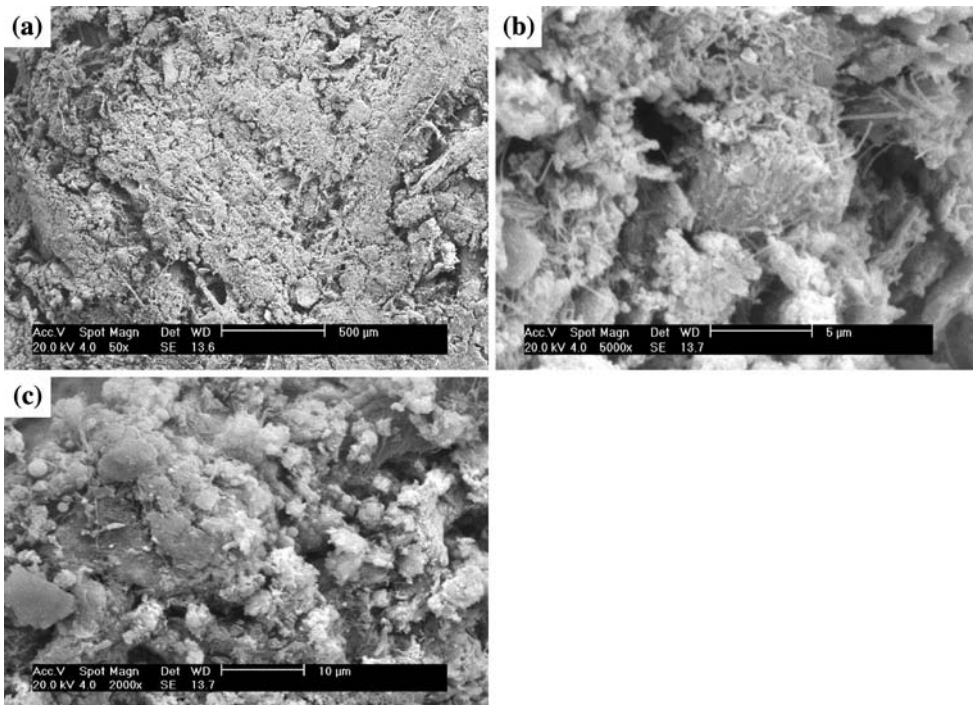

Fig. 8 Bone formation and the degradation after 6 months implantation showing the new formed bone are composed of fibrous tissues, deposited bone apatite and degraded particles

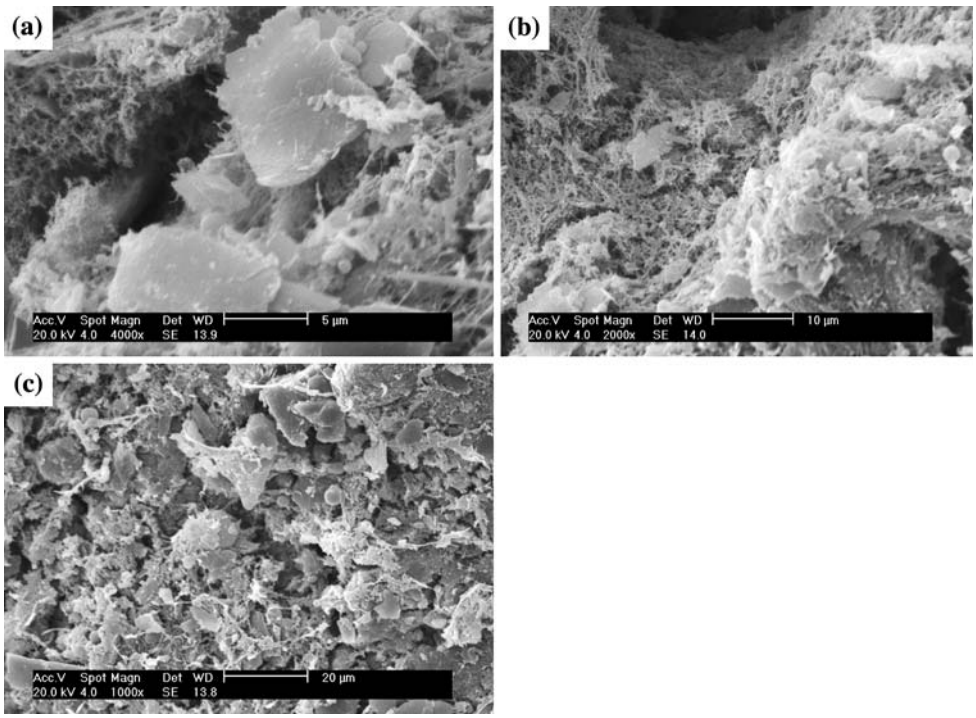

Fig. 9 SEM micrographs of the β-TCP scaffold without in vitro cell culture after implantation for 6 months

the degradation properties of the β-TCP [24]. The interstitial ions of the Na^{+}, Mg^{2+} ions into the β-TCP structure may decrease the structure stability of the material that can promote the degradation of the β-TCP crystals and therefore provide a high calcium and phosphorous ions concentration to deposit apatite bone mineral crystals on the extracellular matrix collagen fibers that secreted by the osteoblast cells and then provided a fast bone formation.

4 Conclusion

In this study the high strength porous β-TCP bone tissue scaffold has been successfully prepared with a highest compressive strength of 4.32 MPa while the porosity is 70% by a solid solution sintering effects of the Na_2O–MgO–CaO–P_2O_5 bioglass without the phase transformation of β-TCP to α-TCP. The improvement effects of the

mechanical properties can be concluded as following: one is the repair effect of the large cracks that formed during the drying process by the liquid bioglass phase at the sintering temperature and the low densification temperature due to the solid solution sintering mechanism that has avoided the high temperature phase transformation of β to α phase, which is negative to the mechanical properties of the β-TCP matrix. Another fact is that the solid solution of the Na^+, Mg^{2+} ions into the β-TCP structure has formed chemical bonding between grain crystals and also has induced a tiny volume expansion that had strengthened the materials' boundary leading to a tighter bonding between the crystals and has induced more transgranular fracture. The effect of the solid solution of the Na^+, Mg^{2+} ions also displayed in the in vivo testing that promoted the degradation of the β-TCP structure which a high ions concentration had formed and consequently had promoted the bone apatite deposition.

Acknowledgement Authors are grateful to the National Nature Science fund (Grant No. 50772072, 30400451) and Shanghai Science and Technology Program (Grant No.07QA14069) for the financial support to this research.

References

1. De groot K, Klein CPAT, Wolke JGC, Blieck-Hogervorst JMA. Handbook of bioactive ceramics. In: Yamamuro T, Hench LL, Wilson J, editors. Calcium phosphate and hydroxyapatite ceramics, vol. 2. Boca Raton, FL: CRC Press; 1990. p.3.
2. Hench LL. Bioceramics. J Am Ceram Soc. 1998;81:1705–28.
3. Kalita SJ, Bhatt HA, Dhamne A. MgO–Na_2O–P_2O_5-based sintering additives for tricalcium phosphate bioceramics. J Am Ceram Soc. 2006;89:875. doi:10.1111/j.1551-2916.2005.00854.x.
4. Gibson IR, Rehman I, Best SM. Characterization of the transformation from calcium-deficient apatite to β-tricalcium phosphate. J Mater Sci Mater Med. 2000;12:799–804. doi:10.1023/A:1008905613182.
5. Deville S, Saiz E, Tomsia AP. Freeze casting of hydroxyapatite scaffolds for bone tissue engineering. Biomaterials. 2006;27(32):5480–9. doi:10.1016/j.biomaterials.2006.06.028.
6. Taboas JM, Maddox RD, Krebsbach PH, Hollister SJ. Indirect solid free form fabrication of local and global porous, biomimetic and composite 3D polymer-ceramic scaffolds. Biomaterials. 2003;24:181–94. doi:10.1016/S0142-9612(02)00276-4.
7. Will J, Melcher R, Treul C, Travitzky N, Kneser U, Polykandriotis E, et al. Porous ceramic bone scaffolds for vascularized bone tissue regeneration. J Mater Sci Mater Med. 2008;19:2781–90.
8. Julia A, Lebugle A. Influence de l'e'tat cristallin sur la solubilite'du magne'sium dans les orthophosphates de calcium. J Solid State Chem. 1990;84(2):342. doi:10.1016/0022-4596(90)90332-R.
9. Famery R, Richard N, Boch P. Preparation of α- and β-tricalcium phosphate ceramics, with and without magnesium addition. Ceram Int. 1994;20:327–36. doi:10.1016/0272-8842(94)90050-7.
10. Ryu HS, Youn HJ, Homg KS, Chang BS, Lee CK, Chung SS. An improvement in sintering property of β-tricalcium phosphate by addition of calcium pyrophosphate. Biomaterials. 2002;23:909–14. doi:10.1016/S0142-9612(01)00201-0.
11. Toriyama M, Kawamura S, Ito Y, Nagae H, Toyama I. Effect of mixed addition of Al_2O_3 and SiO_2 on mechanical strength of sintered β-tricalcium phosphate. J Ceram Soc Jpn. 1988;96(8):837.
12. Itatani K, Takahadi M, Howell FS, Aizawa M. Effect of metal–oxide addition on the sintering of β-calcium orthophosphate. J Mater Sci Mater Med. 2002;13:707–13. doi:10.1023/A:1015754229181.
13. Ryu HS, Youn HJ, Homg KS, Kim SJ, Lee DH, Chang BS, et al. Correlation between MgO doping and sintering characteristics in hydroxyapatite/β-tricalcium phosphate composite. Bioceramics. 2002;14:21.
14. Toriyama M, Kawamura S, Ishida K. Effect of MgO addition on bending strength of sintered beta-tricalcium phosphate prepared by mechanochano chemical synthesis. Yogyo Kyokaishi. 1987;95:822.
15. Yu XZ, Cai S, Zhang Z, Xu GH. Bioactive pyrophosphate glass/beta-tricalcium phosphate composite with high mechanical properties. Mater Sci Eng C. 2008;28:1138–43. doi:10.1016/j.msec.2007.08.001.
16. Cai S, Xu GH, Yu XZ, Zhang WJ, Xiao ZY, Yao KD. Fabrication and biological characteristics of b-tricalcium phosphate porous ceramic scaffolds reinforced with calcium phosphate glass. J Mater Sci Mater Med. 2009;20:351–8. doi:10.1007/s10856-008-3591-2.
17. Boyd D, Carroll G, Towler MR, Freeman C, Farthing P, Brook IM. Preliminary investigation of novel bone graft substitutes based on strontium–calcium–zinc–silicate glasses. J. Mater Sci Mater Med. 2009;20(1):413–20. doi:10.1007/s10856-008-3569-0.
18. Cotton FA, Wilkinson G, Murillo CA, Bochmann M. Advanced inorganic chemistry. 6th ed. New York: Wiley; 1999.
19. Lee BK, Chung SY, Kang SJL. Grain boundary faceting and abnormal grain growth in $BaTiO_3$. Acta Mater. 2000;8(7):1575–80.
20. Anderson MP, Grest GS, Doherty RD, Kang L, Srolovitz DJ. Inhibition of grain growth by second phase particles: three dimensional Monte Carlo computer simulations. Scripta Metall. 1989;23(5):753-8.
21. Ko HC, Han JS, Bachle M, Jang JH, Shina SW, Kim DJ. Initial osteoblast-like cell response to pure titanium and zirconia/alumina ceramics. Dental mateirials. 2007;23(11):1349–55.
22. Lu JX, Flautre B, Anselme K, Hardouin P, Gallur A, Descamps M, et al. Role of interconnections in porous bioceramics on bone recolonization in vitro and in vivo. J Mater Sci: Mater Med. 1999;10:111–20.
23. Hee CK, Jonikas MA, Nicoll SB. Influence of three-dimensional scaffold on the expression of osteogenic differentiation markers by human dermal fibroblasts. Biomaterials. 2006;27:875–84.
24. Okazaki M, Sato M. Computer graphics of hydroxyapatite and beta-tricalcium phosphate. Biomaterials. 1990;11(8):573–8.